As discussed later, our results indicate a possible molecular mechanism for the 5′-GGGA-3′ to 5′-GGA-3′ mutation induced by PhIP.

DNA Polymerases Involved in TLS through the dG-PhIP Adduct—TLS through many DNA lesions requires the action of two different polymerases, an "inserter" and an "extender," the former to perform nucleotide insertions opposite the lesion site and the latter for subsequent extensions (39). The catalytic efficiency of the dCTP-insertion reaction opposite the dG-PhIP adduct by REV1 was found to be more than 2,000-fold greater than that by pol κ (see Tables 2 and 3). This result strongly suggests that REV1 functions *in vivo* as an inserter polymerase for TLS through the dG-PhIP adduct. This insertion step by REV1 is also error free. REV1 has been reported previously to insert dCTP opposite abasic sites and various N2-dG adducts (26, 39–41). However, our current study is the first to show that REV1 inserts dCTP opposite a large size C8-dG adduct. We used a shorter (C-terminal deleted) form of pol κ in our current experiments and an intact pol κ may be more effective for this insertion reaction. As for pol η, a detailed kinetic analysis was not performed. Hence, the possibility cannot be excluded that pol κ and pol η also function as inserter polymerases.

In addition to the Y-family DNA polymerases, DNA polymerase ζ (pol ζ), belonging to the B-family DNA polymerases, is considered to be involved in TLS through various lesions as an extender DNA polymerase (39, 42, 43). We have not carried out a primer extension assay with pol ζ and thus the possibility cannot be completely excluded by our current data that pol ζ functions *in vivo* as an extender polymerase for TLS through the dG-PhIP adduct. In our present study, we provide evidence that pol κ can extend from dC opposite the dG-C8-PhIP adduct *in vitro*. It is, therefore, possible that pol κ, at least partially, functions as an extender polymerase *in vivo* for TLS through the dG-PhIP adduct. Further study about cooperation between two or more DNA polymerases, including pol ζ, is necessary to verify which DNA polymerases are involved in the bypass synthesis through the PhIP lesion.

The catalytic efficiency of pol κ for a dGTP insertion into substrate C-p28 was a little higher than that for dCTP insertions (see Table 2 and Fig. 6*D*). The former generates a single guanine deletion, and the latter is an error-free extension. Consequently, our data suggest that the extension reaction with pol κ from the nucleotide opposite the dG-C8-PhIP adduct causes frequent single-guanine deletions from the GGG stretch. It has been reported that one characteristic feature of pol κ homologs, from bacteria to humans, is their propensity to generate single-base deletions (44–47). The crystal structure of Dpo4, a thermophilic archaea homolog of pol κ, in ternary complexes with DNA and an incoming nucleotide supports the model that a single base deletion by pol κ is generated through a misaligned intermediate complex where the template dG forms an extrahelical looped out structure and the incoming dGTP skips this extrahelical base and pairs with the next template base dC (48) (see supplemental Fig. S6). It is reasonable to speculate therefore that, in the case of TLS through dG-C8-PhIP, mammalian pol κ generates the single guanine deletion via a similar intermediate where the PhIP-adducted dG is looped out and template-primer slippage occurs. However, further analyses for determining whether the one-base skipping of pol κ beyond the lesion observed by us is dependent on the nucleotide placed 5′ to the lesion or not, are necessary to clarify the detailed molecular mechanism underlying one base skipping of pol κ.

Molecular Mechanisms Underlying Mutation Induction by PhIP—We have demonstrated herein by *in vitro* DNA synthesis analyses using oligonucleotide templates containing dG-PhIP that: 1) replicative DNA polymerases stall at the PhIP adduct and cannot perform translesional DNA synthesis beyond this point; 2) REV1 inserts a dC opposite the dG-PhIP with a much higher efficiency than other TLS polymerases, including pol κ and pol η; and 3) pol κ has a potential ability to catalyze an extension reaction from the 5′-dC opposite the adduct and often skips over one dG in the template during this extension step. A working model for the induction of mutations at the PhIP adducts based on the results shown in the present study is illustrated in supplemental Fig. S6. This model could be adopted for other sequences containing a G repeat stretch longer than GGG.

REFERENCES

1. Nagao, M. (2000) in *Food Borne Carcinogens: Heterocyclic Amines* (Nagao, M., and Sugimura, T., eds) pp. 163–196, John Wiley & Sons Ltd., Chichester, UK
2. Schut, H. A., and Snyderwine, E. G. (1999) *Carcinogenesis* **20,** 353–368
3. Felton, J. S., Knize, M. G., Shen, N. H., Lewis, P. R., Andresen, B. D., Happe, J., and Hatch, F. T. (1986) *Carcinogenesis* **7,** 1081–1086
4. Felton, J. S., Jagerstad, M., Knize, M. G., Skog, K., and Wakabayashi, K. (2000) in *Food Borne Carcinogens: Heterocyclic Amines* (Nagao, M., and Sugimura, T., eds) pp. 31–71, John Wiley & Sons Ltd., Chichester, UK
5. Holme, J. A., Wallin, H., Brunborg, G., Søderlund, E. J., Hongslo, J. K., and Alexander, J. (1989) *Carcinogenesis* **10,** 1389–1396
6. Felton, J. S., and Knize, M. G. (1991) *Mutat. Res.* **259,** 205–217
7. Ohgaki, H., Takayama, S., and Sugimura, T. (1991) *Mutat. Res.* **259,** 399–410
8. Ito, N., Hasegawa, R., Sano, M., Tamano, S., Esumi, H., Takayama, S., and Sugimura, T. (1991) *Carcinogenesis* **12,** 1503–1506
9. Sugimura, T., Wakabayashi, K., Nakagama, H., and Nagao, M. (2004) *Cancer Sci.* **95,** 290–299
10. Imaida, K., Hagiwara, A., Yada, H., Masui, T., Hasegawa, R., Hirose, M., Sugimura, T., Ito, N., and Shirai, T. (1996) *Jpn. J. Cancer Res.* **87,** 1116–1120
11. Frandsen, H., Grivas, S., Andersson, R., Dragsted, L., and Larsen, J. C. (1992) *Carcinogenesis* **13,** 629–635
12. Lin, D., Kaderlik, K. R., Turesky, R. J., Miller, D. W., Lay, J. O., Jr., and Kadlubar, F. F. (1992) *Chem. Res. Toxicol.* **5,** 691–697
13. Snyderwine, E. G., Davis, C. D., Nouso, K., Roller, P. P., and Schut, H. A. (1993) *Carcinogenesis* **14,** 1389–1395
14. Schut, H. A., and Herzog, C. R. (1992) *Cancer Lett.* **67,** 117–124
15. Endo, H., Schut, H. A., and Snyderwine, E. G. (1994) *Cancer Res.* **54,** 3745–3751
16. Morgenthaler, P. M., and Holzhäuser, D. (1995) *Carcinogenesis* **16,** 713–718
17. Yadollahi-Farsani, M., Gooderham, N. J., Davies, D. S., and Boobis, A. R. (1996) *Carcinogenesis* **17,** 617–624
18. Okonogi, H., Stuart, G. R., Okochi, E., Ushijima, T., Sugimura, T., Glickman, B. W., and Nagao, M. (1997) *Mutat. Res.* **395,** 93–99
19. Lynch, A. M., Gooderham, N. J., Davies, D. S., and Boobis, A. R. (1998) *Mutagenesis* **13,** 601–605
20. Okochi, E., Watanabe, N., Shimada, Y., Takahashi, S., Wakazono, K., Shirai, T., Sugimura, T., Nagao, M., and Ushijima, T. (1999) *Carcinogenesis* **20,** 1933–1988
21. Kakiuchi, H., Watanabe, M., Ushijima, T., Toyota, M., Imai, K., Weisburger, J. H., Sugimura, T., and Nagao, M. (1995) *Proc. Natl. Acad. Sci.*

U.S.A. **92,** 910–914
22. Takamura-Enya, T., Ishikawa, S., Mochizuki, M., and Wakabayashi, K. (2006) *Chem. Res. Toxicol.* **19,** 770–778
23. Masuda, Y., Suzuki, M., Piao J., Gu, Y., Tsurimoto, T., and Kamiya, K. (2007) *Nucleic Acids Res.* **35,** 6904–6916
24. Masutani, C., Kusumoto, R., Iwai, S., and Hanaoka, F. (2000) *EMBO J.* **19,** 3100–3109
25. Niimi, N., Sassa, A., Katafuchi, A., Grúz, P., Fujimoto, H., Bonala, R. R., Johnson, F., Ohta, T., and Nohmi, T. (2009) *Biochemistry* **48,** 4239–10234246
26. Masuda, Y., and Kamiya, K. (2002) *FEBS Lett.* **520,** 88–92
27. Masuda, Y., Ohmae, M., Masuda, K., and Kamiya, K. (2003) *J. Biol. Chem.* **278,** 12356–12360
28. Sambrook, J., Fritsch, E. F., and Maniatis, T. (1989) *Molecular Cloning: A Laboratory Manual,* 2nd Ed., Cold Spring Harbor Laboratory, Cold Spring Harbor, NY
29. Fukuda, H., and Ohtsubo, E. (1997) *Genes Cells* **2,** 735–751
30. Fukuda, H., Katahira, M., Tsuchiya, N., Enokizono, Y., Sugimura, T., Nagao, M., and Nakagama, H. (2002) *Proc. Natl. Acad. Sci. U.S.A.* **99,** 12685–12690
31. Sugiyama, H., and Saito, I. (1996) *J. Am. Chem. Soc.* **118,** 7063–7068
32. Mozzherin, D. J., Shibutani, S., Tan, C. K., Downey, K. M., and Fisher, P. A. (1997) *Proc. Natl. Acad. Sci. U.S.A.* **94,** 6126–6231
33. Sugimura, T., and Adamson, R. H. (2000) in *Food Borne Carcinogens: Heterocyclic Amines* (Nagao, M., and Sugimura, T., eds) pp. 1–4, John Wiley & Sons Ltd., Chichester, UK
34. Choi, J. Y., Stover, J. S., Angel, K. C., Chowdhury, G., Rizzo, C. J., and Guengerich, F. P. (2006) *J. Biol. Chem.* **281,** 25297–25306
35. Nakagama, H., Ochiai, M., Ubagai, T., Tajima, R., Fujiwara, K., Sugimura, T., and Nagao, M. (2002) *Mutat. Res.* **506–507,** 137–144
36. Nagao, M. (1999) *Mutat. Res.* **431,** 3–12
37. Nagao, M., Ushijima, T., Toyota, M., Inoue, R., and Sugimura, T. (1997) *Mutat. Res.* **376,** 161–167
38. Dashwood, R. H., Suzui, M., Nakagama, H., Sugimura, T., and Nagao, M. (1998) *Cancer Res.* **58,** 1127–1129
39. Prakash, S., Johnson, R. E., and Prakash, L. (2005) *Annu. Rev. Biochem.* **74,** 317–353
40. Nelson, J. R., Lawrence, C. W., and Hinkle, D. C. (1996) *Nature* **382,** 729–731
41. Haracska, L., Prakash, S., and Prakash, L. (2002) *J. Biol. Chem.* **277,** 15546–15551
42. Johnson, R. E., Washington, M. T., Haracska, L., Prakash, S., and Prakash, L. (2000) *Nature* **406,** 1015–1019
43. Haracska, L., Unk, I., Johnson, R. E., Johansson, E., Burgers, P. M., Prakash, S., and Prakash, L. (2001) *Genes Dev.* **15,** 945–954
44. Kim, S. R., Maenhaut-Michel, G., Yamada, M., Yamamoto, Y., Matsui, K., Sofuni, T., Nohmi, T., and Ohmori, H. (1997) *Proc. Natl. Acad. Sci. U.S.A.* **94,** 13792–13797
45. Kobayashi, S., Valentine, M. R., Pham, P., O'Donnell, M., and Goodman, M. F. (2002) *J. Biol. Chem.* **277,** 34198–34207
46. Ogi, T., Kato, T., Jr., Kato, T., and Ohmori, H. (1999) *Genes Cells* **4,** 607–618
47. Ohashi, E., Bebenek, K., Matsuda, T., Feaver, W. J., Gerlach, V. L., Friedberg, E. C., Ohmori, H., and Kunkel, T. A. (2000) *J. Biol. Chem.* **275,** 39678–39684
48. Ling, H., Boudsocq, F., Woodgate, R., and Yang, W. (2001) *Cell* **107,** 91–102

FEBS Letters 583 (2009) 2710–2714

FEBS Letters

journal homepage: www.FEBSLetters.org

Mdmx enhances p53 ubiquitination by altering the substrate preference of the Mdm2 ubiquitin ligase

Koji Okamoto [a,b,c], Yoichi Taya [b,c,1], Hitoshi Nakagama [a,*]

[a] National Cancer Center Research Institute, Early Oncogenesis Research Project, 5-1-1 Tsukiji, Chuo-ku, Tokyo 104-0045, Japan
[b] National Cancer Center Research Institute, Radiobiology Division, 5-1-1 Tsukiji, Chuo-ku, Tokyo 104-0045, Japan
[c] SORST, Japan Science and Technology Corporation, Japan

ARTICLE INFO

Article history:
Received 11 May 2009
Revised 26 June 2009
Accepted 13 July 2009
Available online 18 July 2009

Edited by Noboru Mizushima

Keywords:
Mdmx
Mdm2
p53
Ubiquitination

ABSTRACT

***mdm2* and *mdmx* oncogenes play essential yet non-redundant roles in synergistic inactivation of the tumor suppressor, p53. While Mdm2 inhibits p53 activity mainly by augmenting its ubiquitination, the functional role of Mdmx on p53 ubiquitination remains obscure. In transfected H1299 cells, Mdmx augmented Mdm2-mediated ubiquitination of p53. In in vitro ubiquitination assays, the Mdmx/Mdm2 heteromeric complex, in comparison to the Mdm2 homomer, showed enhanced ubiquitinase activity toward p53 and the reduced auto-ubiquitination of Mdm2. Alteration of the substrate specificity via binding to Mdmx may contribute to efficient ubiquitination and inactivation of p53 by Mdm2.**

Structured summary:
MINT-7219995: *P53* (uniprotkb:P04637) *physically interacts* (MI:0914) with *Ubiquitin* (uniprotkb:P62988) by *anti bait coimmunoprecipitation* (MI:0006)
MINT-7220023: *Ubiquitin* (uniprotkb:P62988) *physically interacts* (MI:0914) with *P53* (uniprotkb:P04637) by *pull down* (MI:0096)

1. Introduction

The p53 tumor suppressor protein plays a central role in preventing tumorigenesis. p53 functions as a sequence-specific transcriptional factor [1,2], and activated p53 exerts its function as a tumor suppressor by inducing numerous target genes [3–6]. In most cancer cells, its activity is lost via alteration of its gene or via other cellular events that inactivate p53 [7–9].

Mdm2 and Mdmx function as two major players in the suppression of p53 activity [10]. Accumulating reports indicate that the major function of Mdm2 in suppressing p53 is attributed to Mdm2-dependent p53 ubiquitination, which triggers proteasomal degradation or nuclear export of p53 [11], although it has been reported that Mdm2 inactivates p53 by other mechanisms [12–15]. Mdm2 possesses a RING finger domain, a protein–protein interaction motif that is found in many eukaryotic proteins and often possesses E3 ubiquitin ligase activity [16]. Indeed, Mdm2 functions as an E3 ubiquitin ligase, and the RING domain of Mdm2 is essential for its ubiquitin ligase activity toward p53 and Mdm2 itself [17–19].

Mdmx shares an extensive structural homology with Mdm2, and forms a heterodimer complex with Mdm2 through their RING finger domains [20,21], yet Mdmx in itself lacks the robust activity of an E3 ubiquitin ligase [22]. Thus, both genetic and biochemical evidence indicates that Mdmx and Mdm2 perform distinct yet co-operative functions in p53 inactivation.

Recent reports suggest that Mdmx may inactivate p53 by augmenting Mdm2-mediated ubiquitination of p53 [23–25]. However, precise mechanism by which Mdmx stimulates p53 ubiquitination by Mdm2 is not yet known.

In this paper, we demonstrated that wild-type Mdmx is capable of enhancing Mdm2-mediated p53 ubiquitination in vivo. Further, the in vitro study using purified Mdm2 or the Mdm2/Mdmx complex revealed that, when complexed with Mdmx, the extent of p53 ubiquitination by Mdm2 was enhanced while poly-ubiquitination of Mdm2 was significantly decreased. We propose that the effect of Mdmx on the preference of the substrate of the Mdm2 ubiquitin ligase plays an important role in effective ubiquitination of p53.

* Corresponding author.
E-mail address: hnakagam@ncc.go.jp (H. Nakagama).
[1] Present address: Cancer Science Institute of Singapore, National University of Singapore, Singapore 117456, Singapore.

0014-5793/$36.00 © 2009 Federation of European Biochemical Societies. Published by Elsevier B.V. All rights reserved.
doi:10.1016/j.febslet.2009.07.021

2. Materials and methods

2.1. DNA transfection

In DNA transfection experiments using H1299 cells, 2 μg of DNA and 4 μl of Lipofectamine 2000 reagent (Invitrogen) were introduced per 2.0×10^5 cells according to manufacturer's protocol. Cells were then incubated for 20 h before harvesting.

2.2. In vivo ubiquitination assay

For detection of p53 conjugated with endogenous ubiquitin, in vivo ubiquitination assays were performed as previously described [26] with some modifications. Transfected H1299 cells were lysed in SDS lysis buffer (50 mM Tris, pH 7.5, 100 mM NaCl, 1% SDS) supplemented with 1 mM DTT and protease inhibitor cocktail (PI) [27], boiled for 10 min, and diluted with ×4 volumes of dilution buffer (50 mM Tris, pH 7.5, 100 mM NaCl, 1.25% Triton X-100) supplemented with DTT and PI. After sonication of the lysates, p53 was immunoprecipitated with anti-p53 antibody (DO-1). Subsequently the immunoprecipitates were washed three times with 200-NP buffer [27], and analyzed by Western blotting with DO-1 and anti-ubiquitin antibody (FK2, MBL).

For detection of p53 conjugated with transfected $(His)_6$-ubiquitin, transfected H1299 cells were lysed in urea lysis buffer (100 mM NaH2PO4, 10 mM Tris–HCl, pH 8.0, 500 mM NaCl, 10% glycerol, 0.1% Triton X-100, 10 mM imidazole) supplemented with 10 mM β-mercaptoethanol, PI, 5 mM Iodoacetamide, and 1 mg/ml NEM. Proteins conjugated with His-tagged ubiquitin were purified as described before [28], and analyzed by Western blot analysis.

2.3. Protein expression and purification

Flag-tagged Human Mdm2 (Flag-Mdm2) or Human Mdmx RNA was transcribed from the corresponding cDNA using the Wheat Germ Expression Kit (Cell Free Science, Japan). Subsequently, the Flag-Mdm2 RNA alone or in combination with an excess amount of the Mdmx RNA was used for in vitro translation with wheat germ lysate (Cell Free Science) according to the manufacturer's instructions. Flag-Mdm2 or the Flag-Mdm2/Mdmx complex was then purified on agarose conjugated with anti-Flag antibody.

2.4. In vitro ubiquitination assay

In vitro ubiquitination assays were performed as previously described with some modifications [29]. Approximately 100 ng of Flag-Mdm2 or the Flag-Mdm2/Mdmx complex were mixed with the following purified components; 8 ng of GST-p53, 10 ng of E1 (Boston Biochem), 80 ng of E2 (UbcH5b, Boston Biochem), 3 μg of His-ubiquitin (Calbiochem), or methylated ubiquitin (Boston Biochem). In experiments shown in Fig. 4D, ^{125}I-ubiquitin (Perkin–Elmer) was included in the reaction mixture. These components were incubated in a reaction buffer (40 mM Tris–HCl, pH 7.5, 5 mM $MgCl_2$, 10 mM NaCl) in the presence of 2 mM Mg–ATP at 37 °C for the indicated times. After the reactions were terminated by adding SDS sample buffer, ubiquitinated proteins were separated in SDS–PAGE gels and detected by Western blot analyses or autoradiography.

3. Results

3.1. Wild-type Mdmx was capable of enhancing p53 ubiquitination in the presence of Mdm2 in vivo

Recently, we demonstrated that the non-phosphorylatable, active form of Mdmx augments p53 ubiquitination mediated by wild-type Mdm2 in transfected H1299 cells [30]. In order to determine whether wild-type Mdmx cooperates with Mdm2 to induce ubiquitination of p53 as well, wild-type Mdmx (Mdmx-wt) or the non-phosphorylated form of Mdmx (Mdmx-3A) was transfected together with Mdm2 into H1299 cells, and conjugation of p53 with endogenous ubiquitin was examined by Western blot analyses (Fig. 1). As expected from previous observation [30], Mdmx-3A, which is resistant to Mdm2-mediated ubiquitination and degradation, was expressed at higher levels than wild-type Mdmx (Fig. 1, lanes 2 and 3). p53 ubiquitination induced by Mdm2 was enhanced in the presence of co-transfected wild-type Mdmx (Fig. 1, lanes 5 and 8), indicating that wild-type Mdmx is capable of stimulating Mdm2-mediated ubiquitination of p53,

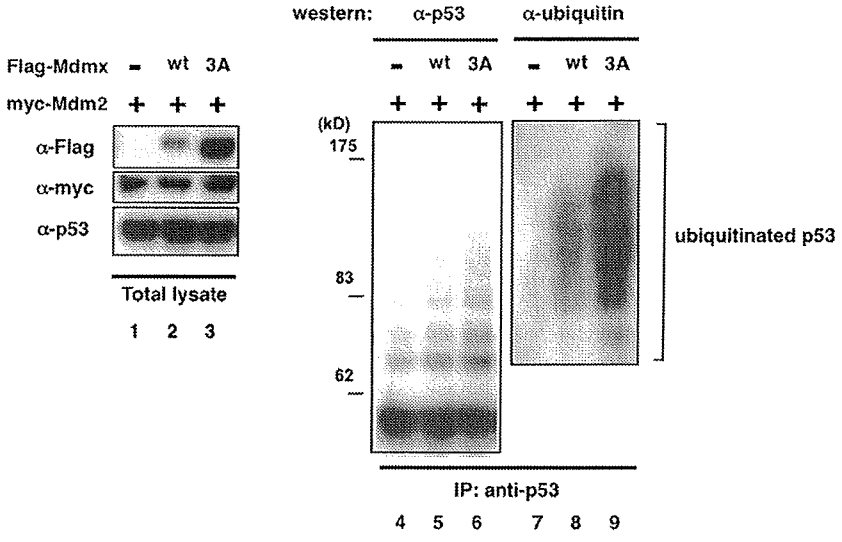

Fig. 1. Mdmx cooperates with Mdm2 to induce p53 ubiquitination. HA-p53 (0.15 mg) and either 0.4 mg of the control vector, wild-type Flag-Mdmx, or the Flag-Mdmx-3A mutant were transfected into H1299 cells in the presence of 0.2 mg of Myc-Mdm2. The total amount of transfected DNA was adjusted to 2 μg with pBluescript plasmid (Stratagene). Twenty hours after transfection, lysates prepared under denaturing conditions were used for immunoprecipitaiton with anti-p53 (DO-1) antibody. The immunoprecipitates were then used for Western blot analyses with DO-1 (left panel, and right bottom panel for low exposure) and with anti-ubiquitin antibody (right panel). Amounts of immunoprecipitates used for Western were normalized such that an equal amount of non-ubiquitinated p53 was loaded in each lane.

although the extent of the stimulation is less than that induced by the non-phosphorylatable mutant (Fig. 1, lanes 6 and 9).

3.2. Mutation at the C-terminal ubiquitinated lysines largely abolished p53 ubiquitination by Mdmx

It has been documented that Mdm2 ubiquitinates p53 at the six C-terminal lysines, the integrity of which are required for its nuclear export [31,32]. We created a mutant p53 in which all six lysines at the C-terminal domain (Fig. S1) were substituted by arginine (p53-K6R), and introduced wild-type p53 or the K6R mutant into H1299 cells together with Mdm2 in the presence or absence of Mdmx-3A. Examination of p53 ubiquitination in vivo revealed that the K6R mutation eliminates a majority of p53 ubiquitination enhanced by Mdmx (Fig. S2), indicating the six lysines were major sites for Mdmx-dependent ubiquitination.

3.3. Association of Mdmx with Mdm2 augments the ability of Mdm2 to ubiquitinate p53 and inhibits poly-ubiquitination of Mdm2 in vitro

In order to determine whether Mdmx enhances Mdm2-dependent ubiquitination of p53 via direct association with Mdm2, we next performed in vitro ubiquitination assays using purified recombinant proteins of Mdm2 or an Mdm2/Mdmx complex (see Section 2). Silver staining of the purified proteins indicated that the co-purified Mdmx formed a complex with Mdm2 at approximately a 1:1 molar ratio (Fig. 2A, right panel).

In order to determine the effect of the association with Mdmx on the activity of E3 ubiquitin ligase of Mdm2, homomeric Mdm2 or the Mdmx/Mdm2 complex was incubated with E1, E2 (UbcH5b), GST-p53, and ubiquitin, and time-course analyses of the ubiquitination of p53 and auto-ubiquitination of Mdm2 were simultaneously performed. The complex formation of Mdm2 with Mdmx-3A or with wild-type Mdmx resulted in an increase of p53 ubiquitination (Fig. 2B and C). In contrast, the Mdmx/Mdm2 complex showed a marked decrease in poly-ubiquitinated forms of Mdm2 in comparison to homomeric Mdm2 (Fig. 2B and C), indicating that the association with Mdmx-3A augments Mdm2-dependent p53 ubiquitination while it inhibits poly-ubiquitination of Mdm2.

3.4. Mdmx inhibits ubiquitination of the Mdm2-containing enzymatic complex

In order to confirm that Mdmx inhibits auto-ubiquitination of Mdm2, in vitro ubiquitination assays of the Mdm2 homomer or the Mdm2/Mdmx complex were performed in the presence of

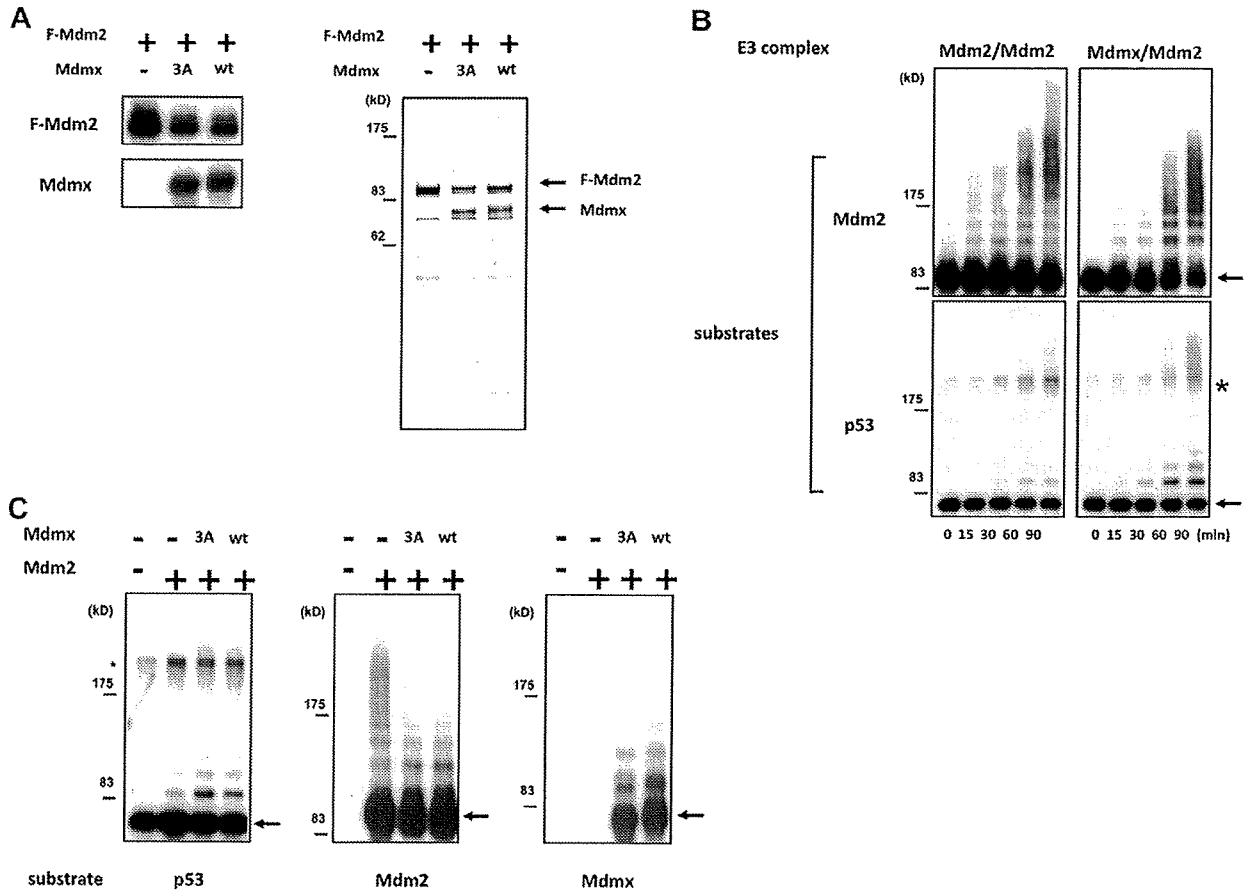

Fig. 2. Association of Mdmx with Mdm2 augments the activity of Mdm2 to ubiquitinate p53 and inhibits auto-ubiquitination of Mdm2 in vitro. (A) Purification of Mdm2 and the Mdm2/Mdmx complex. Flag-tagged Mdm2 was translated alone, or co-translated with Mdmx-3A or wild-type Mdmx in wheat germ lysates, as described in Section 2. The purified proteins were separated by10% SDS–PAGE, and detected by silver staining (right panel), or by Western blotting analyses with anti-Flag antibody (M2) or anti-Mdmx antibody (D-19) (left panel). (B) *In vitro* ubiquitination assays were performed with purified Mdm2 or Mdmx-3A/Mdm2. Ubiquitination reactions were terminated at the indicated times, and the extent of p53 ubiquitination and Mdm2 auto-ubiquitination was evaluated by Western blot analyses with anti-Flag antibody or anti-p53 antibody. The position of non-ubiquitinated substrates is designated by arrows. (C) In vitro ubiquitination assays were performed as described in (B), and the ubiquitination reactions were terminated after 30 min. Ubiquitination of Mdmx, p53, and Mdm2 was evaluated by Western blot analyses.

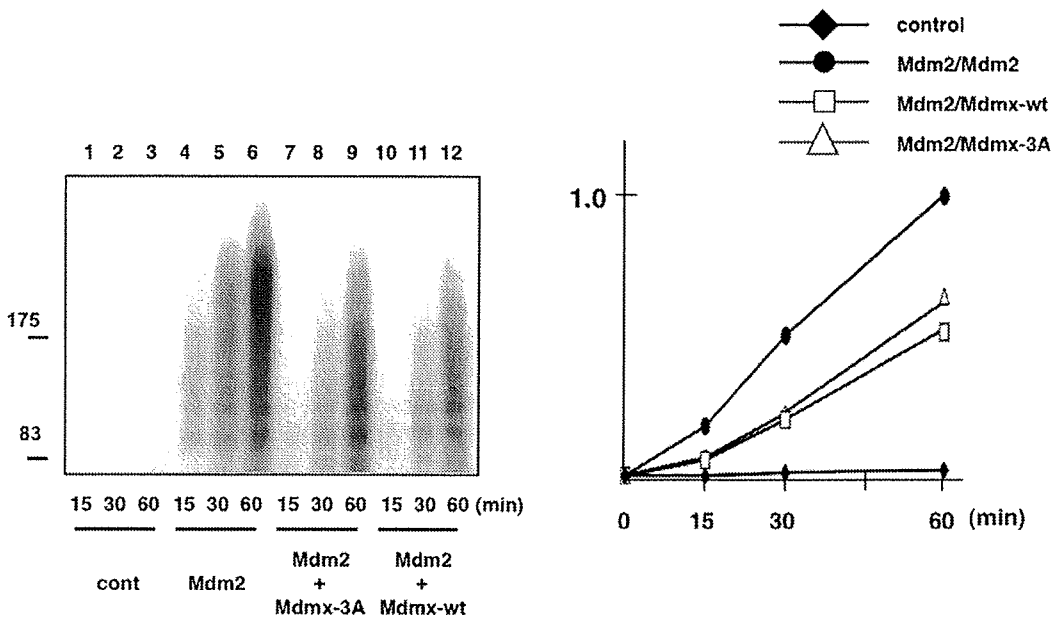

Fig. 3. In vitro ubiquitination reaction was performed as described in Fig. 2C, except that ^{125}I-labeled ubiquitin was included in the reaction. (left panel) Ubiquitinated Mdm2 or Mdm2/Mdmx was separated by 10% SDS–PAGE, and detected by autoradiography. Note that the ladder represents a mixture of ubiquitination of Mdm2 and Mdmx in lanes 7–12 (left panel). Levels of the ubiquitination were quantified and relative levels of ubiquitination were plotted (right panel).

^{125}I-labeled ubiquitin. Quantification of ubiquitin attached to the enzymatic complexes demonstrated that the auto-ubiquitination of the Mdm2 was indeed hindered by the complex formation with either wild-type Mdmx or Mdmx-3A (Fig. 3). Thus, the complex formation of Mdm2 with Mdmx affects the preference for the substrate of the Mdm2 ubiquitin ligase.

3.5. Mdmx stimulates Mdm2-dependent mono-ubiquitination of p53

It has been documented that poly-ubiquitination of p53 induces its degradation, while its mono-ubiquitnation stimulates nuclear export of p53 [33]. Because Mdmx does not significantly contribute to p53 degradation [34], we attempted to determine whether Mdmx stimulates mono-ubiquitination of p53 rather than its poly-ubiquitination. Mdm2 and p53 were introduced into H1299 cells together with His-Ub-K7R, $(His)_6$-tagged mutant ubiquitin which is not capable of forming a ladder of poly-ubiquitination due to arginine substitution in all seven lysine residues [29]. Subsequently, His-Ub-K7R was purified from lysates that were prepared from transfected cells, and p53 conjugated with His-Ub-7KR was detected by Western blot analyses with anti-p53 antibody. The introduction of wild-type Mdmx augmented mono-ubiquitination of p53 (Fig. 4, lane 2), and the Mdmx-3A mutation further enhanced the p53 mono-ubiquitination (Fig. 4, lane 3).

In order to determine whether Mdmx stimulates Mdm2-dependent mono-ubiquitination of p53 in vitro as well as in vivo, methylated ubiquitin was used instead of wild-type ubiquitin in in vitro ubiquitination assays. Indeed, the Mdmx/Mdm2 complex showed a stronger activity for p53 mono-ubiquitination than the homomeric Mdm2 (Fig. S3). Thus, the formation of a complex with Mdmx augments the activity of Mdm2 to mono-ubiquitinate p53.

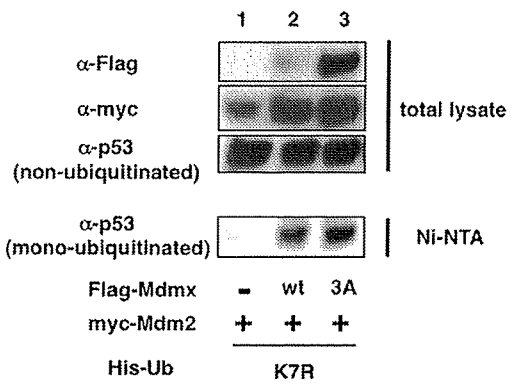

Fig. 4. Mdmx-3A or the control vector was transfected into H1299 cells together with Myc-Mdm2, HA-p53 and the indicated $(His)_6$-tagged ubiquitin K7R mutant. Twenty hours after transfection, cells were lysed with a buffer containing 6 M urea, and normalized lysates that contain equal amounts of non-ubiquitinated p53 were used to purify His-tagged ubiquitin on Ni-NTA agarose (QIAGEN). Ubiquitinated p53 was detected by Western blot analysis with anti-p53 antibody (DO-1).

4. Discussion

In this report, we demonstrated that wild-type Mdmx as well as its non-phosphorylatable mutant cooperates with Mdm2 to stimulate ubiquitination of p53 both in vivo and in vitro. In agreement with our observation, it was reported that Mdmx enhances the activity of Mdm2 as a ubiquitin ligase in vitro [35]. Mdmx complements the catalytic function of mutant Mdm2 proteins that are deficient in the enzymatic activity as a ubiquitin ligase [23–25] and Mdmx/Mdm2 hetero-RING complexes exhibit a greater E3 ligase activity than homomeric Mdm2 [36]. Such effects of Mdmx on Mdm2 should enhance Mdm2-dependent ubiquitination of p53, consistent with the role of Mdmx as an inhibitor of p53.

It was previously reported that Mdmx augments not only auto-ubiquitination of Mdm2 but also the ubiquitin ligase activity of Mdm2 toward p53 [35] in in vitro assays. However, auto-ubiquitination of the Mdm2 ubiquitin ligase negatively affects its activity because poly-ubiquitinated Mdm2 is targeted for proteasome-mediated degradation. Therefore, enhanced ubiquitinase activity of Mdm2 by Mdmx may not be translated into efficient stimulation of p53 ubiquitination if the association of Mdmx to Mdm2 simultaneously leads to stimulation of self-destruction of Mdm2. Our

observation that Mdmx inhibits poly-ubiquitination of Mdm2 while it stimulates p53 ubiquitination may attribute to a mechanism by which Mdmx stimulates Mdm2-dependent p53 ubiquitination without enhanced destruction of Mdm2, thus providing the molecular basis of how Mdmx cooperates with Mdm2 to inhibit p53 activity.

Recently Linke et al. reported the crystal structure of the heterodimer of Mdmx/Mdm2 RING domain, and proposed a model that favors transfer of ubiquitin to Mdmx that does not interact with E2 [37]. This can explain why Mdm2 is not extensively ubiquitinated in the Mdmx/Mdm2 heteromeric complex, thus providing mechanistic basis for reduced ubiquitination of Mdm2 in the Mdmx/Mdm2 complex (Fig. 2). It is noteworthy that, in in vitro ubiquitination assays, the levels of Mdm2 ubiquitination in the homomeric Mdm2 are higher than combined levels of ubiquitination of Mdm2 and Mdmx in the heteromeric complex (Fig. 3). Therefore, it is likely that Mdmx is relatively resistant to ubiquitination by bound Mdm2, unless Mdmx undergoes specific modification such as phosphorylation [27].

It is not clear at this moment how Mdmx stimulates Mdm2-mediated ubiquitination of p53. Mdm2 bound to Mdmx may position its catalytic domain more closer to the C-terminal domain of p53 than homomeric Mdm2, resulting in enhanced p53 ubiquitination. Alternatively, Mdm2 or Mdmx may compete with p53 as a substrate for Mdm2, and relative resistance of Mdmx against ubiquitination by bound Mdm2 may translate into facilitated p53 ubiquitination. Presumably, these two possibilities are not mutually exclusive, and combined effects of Mdmx on Mdm2-mediated ubiquitination may serve to stimulate ubiquitination and inactivation of p53.

Acknowledgements

We thank Aart Jochemsen for helpful suggestions. The His-ubiquitin expression plasmids were kind gifts from Wei Gu. We thank Kenji Kashima and Chihiro Ohtsubo for experimental assistance. This work was supported by a Grant-in-Aid for Scientific Research from the Ministry of Education, Culture, Sports, Science and Technology of Japan (Y.T and K.O.), a Grant-in-Aid for Third Term Comprehensive Control Research for Cancer from the Ministry of Health, Labor and Welfare, Japan (Y.T.), and the Foundation for Promotion of Cancer Research (K.O.).

Appendix A. Supplementary data

Supplementary data associated with this article can be found, in the online version, at doi:10.1016/j.febslet.2009.07.021.

References

[1] Levine, A.J. (1997) P53, the cellular gatekeeper for growth and division. Cell 88, 323–331.
[2] Laptenko, O. and Prives, C. (2006) Transcriptional regulation by p53: one protein, many possibilities. Cell Death Differ. 13, 951–961.
[3] Levine, A.J., Hu, W. and Feng, Z. (2006) The P53 pathway: what questions remain to be explored? Cell Death Differ. 13, 1027–1036.
[4] Oren, M. (2003) Decision making by p53: life, death and cancer. Cell Death Differ. 10, 431–442.
[5] Ko, L.J. and Prives, C. (1996) P53: puzzle and paradigm. Genes Dev. 10, 1054–1072.
[6] Vogelstein, B., Lane, D. and Levine, A.J. (2000) Surfing the p53 network. Nature 408, 307–310.
[7] Lozano, G. and Zambetti, G.P. (2005) What have animal models taught us about the p53 pathway? J. Pathol. 205, 206–220.
[8] Vousden, K.H. and Lu, X. (2002) Live or let die: the cell's response to p53. Nat. Rev. Cancer 2, 594–604.
[9] Olivier, M., Eeles, R., Hollstein, M., Khan, M.A., Harris, C.C. and Hainaut, P. (2002) The IARC TP53 database: new online mutation analysis and recommendations to users. Hum. Mutat. 19, 607–614.
[10] Marine, J.C., Francoz, S., Maetens, M., Wahl, G., Toledo, F. and Lozano, G. (2006) Keeping p53 in check: essential and synergistic functions of Mdm2 and Mdm4. Cell Death Differ. 13, 927–934.
[11] Michael, D. and Oren, M. (2003) The p53-Mdm2 module and the ubiquitin system. Semin. Cancer Biol. 13, 49–58.
[12] Momand, J., Zambetti, G.P., Olson, D.C., George, D. and Levine, A.J. (1992) The mdm-2 oncogene product forms a complex with the p53 protein and inhibits p53-mediated transactivation. Cell 69, 1237–1245.
[13] Oliner, J.D., Pietenpol, J.A., Thiagalingam, S., Gyuris, J., Kinzler, K.W. and Vogelstein, B. (1993) Oncoprotein MDM2 conceals the activation domain of tumour suppressor p53. Nature 362, 857–860.
[14] Ito, A., Lai, C.H., Zhao, X., Saito, S., Hamilton, M.H., Appella, E. and Yao, T.P. (2001) P300/CBP-mediated p53 acetylation is commonly induced by p53-activating agents and inhibited by MDM2. Embo J. 20, 1331–1340.
[15] Kobet, E., Zeng, X., Zhu, Y., Keller, D. and Lu, H. (2000) MDM2 inhibits p300-mediated p53 acetylation and activation by forming a ternary complex with the two proteins. Proc. Natl. Acad. Sci. USA 97, 12547–12552.
[16] Joazeiro, C.A. and Weissman, A.M. (2000) RING finger proteins: mediators of ubiquitin ligase activity. Cell 102, 549–552.
[17] Fang, S., Jensen, J.P., Ludwig, R.L., Vousden, K.H. and Weissman, A.M. (2000) Mdm2 is a RING finger-dependent ubiquitin protein ligase for itself and p53. J. Biol. Chem. 275, 8945–8951.
[18] Honda, R. and Yasuda, H. (2000) Activity of MDM2, a ubiquitin ligase, toward p53 or itself is dependent on the RING finger domain of the ligase. Oncogene 19, 1473–1476.
[19] Honda, R., Tanaka, H. and Yasuda, H. (1997) Oncoprotein MDM2 is a ubiquitin ligase E3 for tumor suppressor p53. FEBS Lett. 420, 25–27.
[20] Tanimura, S., Ohtsuka, S., Mitsui, K., Shirouzu, K., Yoshimura, A. and Ohtsubo, M. (1999) MDM2 interacts with MDMX through their RING finger domains. FEBS Lett. 447, 5–9.
[21] Sharp, D.A., Kratowicz, S.A., Sank, M.J. and George, D.L. (1999) Stabilization of the MDM2 oncoprotein by interaction with the structurally related MDMX protein. J. Biol. Chem. 274, 38189–38196.
[22] Stad, R., Little, N.A., Xirodimas, D.P., Frenk, R., van der Eb, A.J., Lane, D.P., Saville, M.K. and Jochemsen, A.G. (2001) Mdmx stabilizes p53 and Mdm2 via two distinct mechanisms. EMBO Rep. 2, 1029–1034.
[23] Singh, R.K., Iyappan, S. and Scheffner, M. (2007) Hetero-oligomerization with MdmX rescues the ubiquitin/Nedd8 ligase activity of RING finger mutants of Mdm2. J. Biol. Chem. 282, 10901–10907.
[24] Uldrijan, S., Pannekoek, W.J. and Vousden, K.H. (2007) An essential function of the extreme C-terminus of MDM2 can be provided by MDMX. Embo J. 26, 102–112.
[25] Poyurovsky, M.V., Priest, C., Kentsis, A., Borden, K.L., Pan, Z.Q., Pavletich, N. and Prives, C. (2007) The Mdm2 RING domain C-terminus is required for supramolecular assembly and ubiquitin ligase activity. Embo J. 26, 90–101.
[26] Carter, S., Bischof, O., Dejean, A. and Vousden, K.H. (2007) C-terminal modifications regulate MDM2 dissociation and nuclear export of p53. Nat. Cell Biol. 9, 428–435.
[27] Okamoto, K., Kashima, K., Pereg, Y., Ishida, M., Yamazaki, S., Nota, A., Teunisse, A., Migliorini, D., Kitabayashi, I., Marine, J.C., Prives, C., Shiloh, Y., Jochemsen, A.G. and Taya, Y. (2005) DNA damage-induced phosphorylation of MdmX at serine 367 activates p53 by targeting MdmX for Mdm2-dependent degradation. Mol. Cell Biol. 25, 9608–9620.
[28] de Graaf, P., Little, N.A., Ramos, Y.F., Meulmeester, E., Letteboer, S.J. and Jochemsen, A.G. (2003) Hdmx protein stability is regulated by the ubiquitin ligase activity of Mdm2. J. Biol. Chem. 278, 38315–38324.
[29] Li, M., Brooks, C.L., Wu-Baer, F., Chen, D., Baer, R. and Gu, W. (2003) Mono- versus polyubiquitination: differential control of p53 fate by Mdm2. Science 302, 1972–1975.
[30] Ohtsubo, C., Shiokawa, D., Kodama, M., Gaiddon, C., Nakagama, H., Jochemsen, A.G., Taya, Y. and Okamoto, K. (2009) Cytoplasmic tethering is involved in synergistic inhibition of p53 by Mdmx and Mdm2. Cancer Sci.
[31] Gu, J., Nie, L., Wiederschain, D. and Yuan, Z.M. (2001) Identification of p53 sequence elements that are required for MDM2-mediated nuclear export. Mol. Cell Biol. 21, 8533–8546.
[32] Lohrum, M.A., Woods, D.B., Ludwig, R.L., Balint, E. and Vousden, K.H. (2001) C-terminal ubiquitination of p53 contributes to nuclear export. Mol. Cell Biol. 21, 8521–8532.
[33] Shmueli, A. and Oren, M. (2004) Regulation of p53 by Mdm2: fate is in the numbers. Mol. Cell 13, 4–5.
[34] Toledo, F., Krummel, K.A., Lee, C.J., Liu, C.W., Rodewald, L.W., Tang, M. and Wahl, G.M. (2006) A mouse p53 mutant lacking the proline-rich domain rescues Mdm4 deficiency and provides insight into the Mdm2-Mdm4-p53 regulatory network. Cancer Cell 9, 273–285.
[35] Linares, L.K., Hengstermann, A., Ciechanover, A., Muller, S. and Scheffner, M. (2003) HdmX stimulates Hdm2-mediated ubiquitination and degradation of p53. Proc. Natl. Acad. Sci. USA 100, 12009–12014.
[36] Kawai, H., Lopez-Pajares, V., Kim, M.M., Wiederschain, D. and Yuan, Z.M. (2007) RING domain-mediated interaction is a requirement for MDM2's E3 ligase activity. Cancer Res. 67, 6026–6030.
[37] Linke, K., Mace, P.D., Smith, C.A., Vaux, D.L., Silke, J. and Day, C.L. (2008) Structure of the MDM2/MDMX RING domain heterodimer reveals dimerization is required for their ubiquitylation in trans. Cell Death Differ.

Gene Therapy (2009), 1–10

www.nature.com/gt

ORIGINAL ARTICLE

Visualization of in vivo *electroporation-mediated transgene expression in experimental tumors by optical and magnetic resonance imaging*

W Aung[1,3], S Hasegawa[1,3], M Koshikawa-Yano[1], T Obata[2], H Ikehira[2], T Furukawa[1], I Aoki[2] and T Saga[1]

[1]*Diagnostic Imaging Group, Molecular Imaging Center, National Institute of Radiological Sciences, Chiba, Japan and* [2]*Biophysics Group, Molecular Imaging Center, National Institute of Radiological Sciences, Chiba, Japan*

In vivo *electroporation (EP) is an efficient method for effective gene transfer and is highly expected for application in anticancer gene therapy. Non-invasive monitoring of gene transfer/expression is critical for optimal gene therapy. Here we report* in vivo *optical and high-field magnetic resonance imaging (MRI) of EP-mediated transgene expression in a tumor model. Initially, we observed spatio-temporal change in* in vivo *EP-mediated transgene expression by optical imaging using red fluorescence protein (RFP) as a reporter gene. Next, we constructed a dual-reporter plasmid carrying a gene-encoding MRI reporter ferritin heavy chain and* RFP *gene to visualize the intratumoral transgene expression by dual modality. Cells transfected with this plasmid showed lower signal intensity on* in vitro T_2*-weighted cellular MRI and quantitatively increased the transverse relaxation rate (*$1/T_2$*) compared with control cells. After conducting* in vivo *EP in an experimental tumor, the plasmid-injected region showed both fluorescent emissions in optical imaging and detectably lowered signal on* T_2*-weighted MRI. The correlative immunohistological findings confirmed that both the reporter transgenes were co-expressed in this region. Thus, our strategy provides a platform for evaluating EP-mediated cancer gene therapy easily and safely without administering contrast agent or substrate.*
Gene Therapy advance online publication, 21 May 2009; doi:10.1038/gt.2009.55

Keywords: in vivo *electroporation; transgene expression;* in vivo *optical imaging; magnetic resonance imaging*

Introduction

Gene therapy is a novel treatment approach still under development, with several trials to cure diseases, such as monogenetic disorder and malignant disease having been carried out.[1,2] There are various methods for gene delivery and, currently *in vivo* gene transfer is on the basis of two ways: viral delivery and non-viral delivery. The former, generally, is a relatively efficient means of introducing a therapeutic gene to target cells. However, the method has some disadvantages, as there exists the potential for immunogenicity, random insertion and its mutagenesis in the genome, uncontrollable chronic expression of the gene, risk of systemic spread, and the fact that the quality control of viral particles for *in vivo* administration is a laborious and expensive protocol.[3] In contrast, non-viral gene delivery is believed to be safer than viral delivery, and it has been shown that efficient and long-term expression could be expected.[4,5]

Correspondence: Dr S Hasegawa or Dr W Aung, Diagnostic Imaging Group, Molecular Imaging Center, National Institute of Radiological Sciences, Anagawa 4-9-1, Inage-ku, Chiba 263-8555, Japan.
E-mails: shase@nirs.go.jp or winn@nirs.go.jp
[3]These authors contributed equally to this work.
Received 30 September 2008; revised 6 January 2009; accepted 6 January 2009

In vivo electroporation (EP) is a method that has emerged to facilitate gene delivery of naked plasmid DNA *in vivo*.[6] It has been used in the laboratory for gene delivery to cells *in vitro* or *in vivo*, and is recently receiving much attention in cancer gene therapy as a clinically applicable method for enhancing gene delivery, based on it being carried out safely and easily with low cost.[7–9] In this method, plasmid DNA is injected into target tissue after which a series of electric pulses that induce temporary and reversible breakdown of cell membrane and pore formation is conducted to augment DNA transport into the cells. It has been applied to not only accessible surface tissue but also to deep tissues.[10] Since the first application of the *in vivo* delivery of chemotherapeutic agents to solid tumor, study of the delivery of plasmid DNA to cancer by EP has grown tremendously. Many earlier studies have shown that intratumoral gene delivery by *in vivo* EP strongly inhibits tumor growth and generates systemic immunity against tumor in experimental models.[11–15] Furthermore, a clinical trial for melanoma treatment using *in vivo* EP has been started.[6] Like other gene delivery methods, non-invasive monitoring of *in vivo* EP-mediated transgene expression of the introduced gene is a critical issue for optimizing the protocol and ensuring efficacy of the treatment. However, non-invasive methods of monitoring EP-mediated transgene expression *in vivo* are not yet well established.

An *in vivo* molecular imaging technique with reporter gene has been used for the non-invasive detection of gene expression, providing information regarding the location and duration of therapeutic gene expression and even quantification of the expression level.[16,17] Reporter gene imaging for different imaging modalities, such as optical, magnetic resonance imaging (MRI) and positron emission tomography have been developed, and the techniques and protocols are being refined rapidly. It has been suggested that *in vivo* reporter gene imaging would be effective for the non-invasive monitoring of gene expression in gene therapy.[18–21]

The aim of this work was to develop a simple, reliable and safe method to visualize transgene expression in tumors mediated by *in vivo* EP in preclinical tumor models for the design of more rational gene therapy. Here, we report *in vivo* optical imaging and 7-T MRI of intratumoral transgene expression mediated by *in vivo* EP, using the corresponding reporter genes *red fluorescence protein* (*RFP*) and *ferritin heavy chain* (*FHC*), respectively.

Results and discussion

In vivo *optical imaging of transgene expression in tumor mediated by* in vivo *electroporation*

We initially sought to determine whether *in vivo* EP enhanced gene delivery into experimental tumors. For this purpose, we constructed pRFP, a plasmid DNA encoding a red fluorescence protein (RFP), DsRed-Express, transcribed by a composite promoter that combines the cytomegalovirus (CMV) immediate early enhancer and a modified chicken β-actin (CAG) promoter.[22] CAG promoter is more efficient than the classical CMV promoter that is often silenced during the establishment of cell lines that stably express the desired transgene.[23] We used plate-and-fork-type electrodes for *in vivo* EP based on the fact that this type was reported to be more effective for gene transfer than needle-type and plate-and-plate-type electrodes.[24,25] We injected a naked form of the plasmid DNA directly into 293T subcutaneous tumors in nude mice and then conducted EP in a tumor on the right, but not on the left side. *In vivo* optical imaging showed that the efficiency of plasmid delivery into the tumor was clearly different. In the tumor subjected to *in vivo* EP, RFP expression was easily detected, whereas fluorescence emission was nearly absent in the tumor subjected to plasmid injection only (Figure 1a), suggesting that *in vivo* EP enhances gene delivery *in vivo*. We then investigated the temporal change in the level of gene expression mediated by *in vivo* EP in the tumor models using serial optical imaging. *In vivo* EP-mediated DsRed RFP expression was visualized even on day 1 (Figure 1b), gradually increased up to its maximal level on about day 6 and decreased thereafter. More longitudinal monitoring of DsRed RFP expression showed that localized gene expression could be observed for over 2 weeks (Figure 1c). In some cases, it was detectable for even longer than 3 weeks (data not shown). Quantified fluorescent intensities are shown in bar graphs in Figures 1b and c. This kinetic pattern of expression was similar to that observed by Pedron-Mazoyer *et al*.[26] when they carried out intradermal EP of 50 μg of DsRed plasmid. Bloquel *et al*.[27] also reported similar kinetics of transgene expression when they injected 60 μg of a plasmid encoding luciferase in the mouse knee joint. In *ex vivo* tumors of killed mice, RFP expression was noted at the plasmid injection site, and RFP-expressing cells scattered in a heterogeneous pattern were clearly evident on confocal fluorescence microscopy of tumor cryosections (Figure 1d). The percentage of cells expressing RFP was estimated to be ~9% in the area where the plasmid DNA was electroporated most efficiently. Taken together, these data confirm that localized trangene expression in tumor is achievable for 2–3 weeks by *in vivo* EP,[28] and provide the basis for a better understanding of the kinetics of transgene expression mediated by *in vivo* EP.

A plasmid DNA construct for dual-modality imaging and alterations in cellular iron metabolism by expression of FHC *gene*

We next sought to visualize the reporter transgene expression mediated by *in vivo* EP by MRI because of its compatibility with clinical use, applicability to repeated use without radiation risk and high spatial resolution without depth limitation.[16] Recently, ferritin or *FHC* gene has been suggested to be a reliable reporter transgene for MRI with a marked effect on solvent MR relaxation rates.[29–31] FHC is an intracellular iron-binding protein that has various biological functions in cells.[32] Overexpression of *FHC* reporter gene in cells causes T_2 (transverse relaxation time) change in its expression site without the exogenous administration of contrast agents. It has been assumed that this is on the basis of the redistribution of intracellular iron and that FHC reporter activation transiently lowers the labile iron pool in cells and augments iron uptake, probably through transferrin receptor (TfR) upregulation to compensate for iron deficiency. We chose the *FHC* gene as MR reporter gene because of its favorable reproducibility and lesser toxicity than other reporters, and because contrast agents would not be needed.[29–31,33] We also chose the use of *in vivo* optical imaging to easily evaluate gene delivery and determine the location of transgene expression in tumors. Therefore, we constructed pFHC–RFP, a bicistronic mammalian expression vector carrying human FHC cDNA and a gene encoding DsRed-Express placed downstream of an internal ribosome entry site (IRES) of the encephalomyocarditis virus (Figure 2a). The IRES sequence allowed the coordinated expression of two reporter genes transcribed by a single CAG promoter, enabling us to check the FHC reporter expression in cells by red fluorescence. As control vector, we created pX-RFP, in which IRES linked-DsRed Express gene was conserved but *FHC* gene was inserted in reverse direction. The 293T cells were transfected with pFHC–RFP or pX-RFP using lipofection. Under fluorescence microscopy, both transfected cells emitted detectable red fluorescence, whereas no fluorescence was observed in the cells without transfection (Figure 2a). Western blot analysis showed that a low level of endogenous FHC protein was expressed in 293T cells and that FHC reporter protein was robustly translated in cells with pFHC–RFP, but hardly with pX-RFP (Figure 2a). We investigated the temporal change in RFP expression in pFHC–RFP-transfected cells (Figure 2b). RFP expression was first visualized at 12–24 h, gradually increased up to its maximal level at 96 h after transfection and decreased

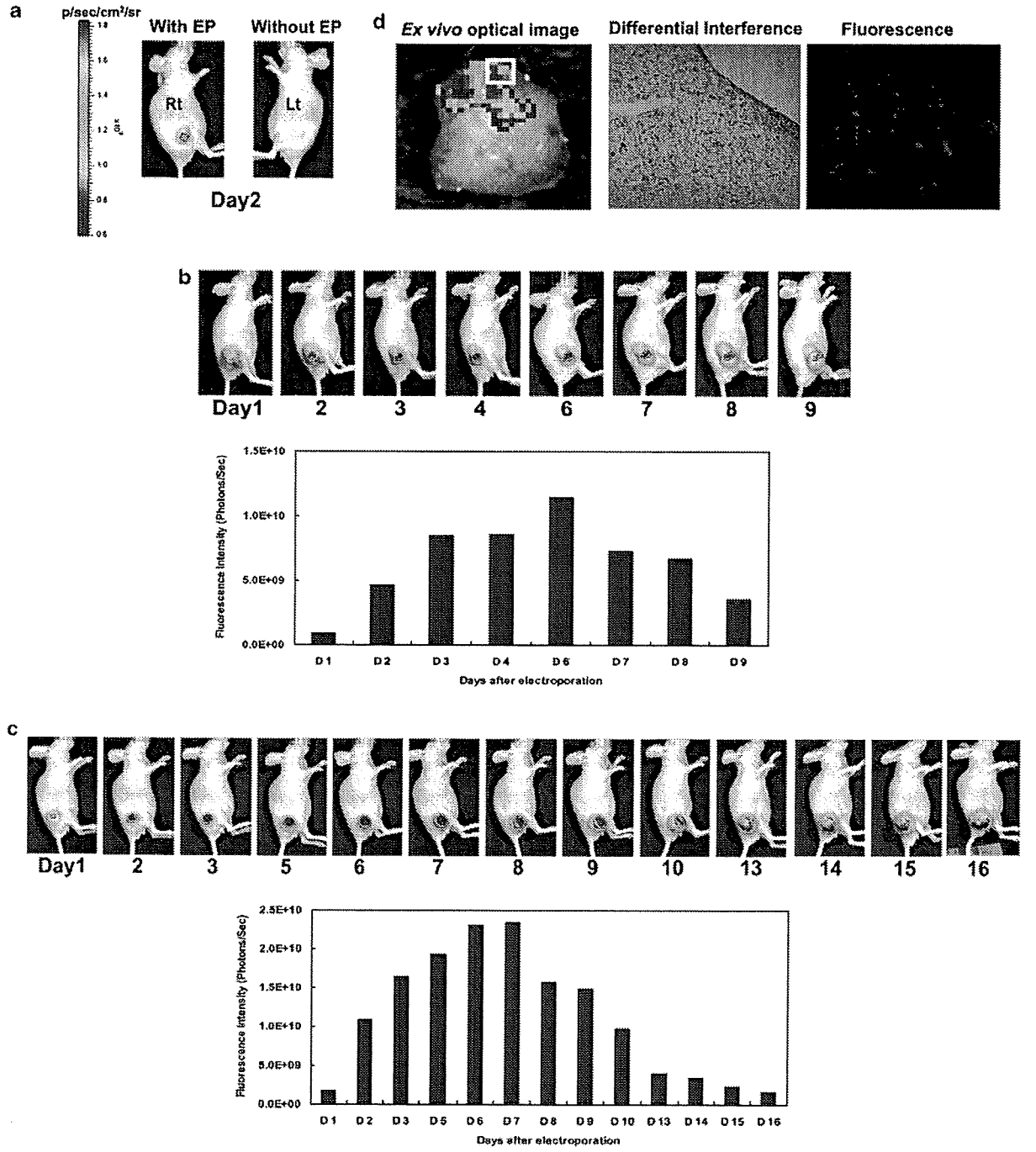

Figure 1 Monitoring of electroporation (EP)-mediated transgene expression by *in vivo* optical imaging. (a) Comparison of transfection efficiency with and without *in vivo* EP in tumor models. Red fluorescence emission was detected in the tumor on the right side (Rt, with EP), whereas the tumor on the left side (Lt, without EP) showed only very faint light emission. (b) Representative images of tumor transfected with pRFP by *in vivo* EP. Days after EP are indicated under the images. Red fluorescence protein (RFP) expression was detected even on day 1, and gradually increased up to the maximal level on around day 6. Images were adjusted to the same scale. Columns, fluorescence intensities quantified in photons per sec. In the image of day 9, a red dotted line encircles the part of the tumor shown in panel d. (c) Representative images for longitudinal monitoring of localized, long-term RFP expression in a tumor followed for more than 2 weeks. Columns, fluorescence intensities detected on indicated days. Scale bar for images in panel b and c was shown in a. (d) *Ex vivo* optical imaging confirmed red fluorescence emission from the plasmid injection site in the tumor. The inset indicates the area shown in differential interference and fluorescence images of tumor cryosection (10 μm). Magnification, × 20. On confocal laser microscopy of tumor sections, red fluorescent cells were visualized as non-homogeneous scattered pattern.

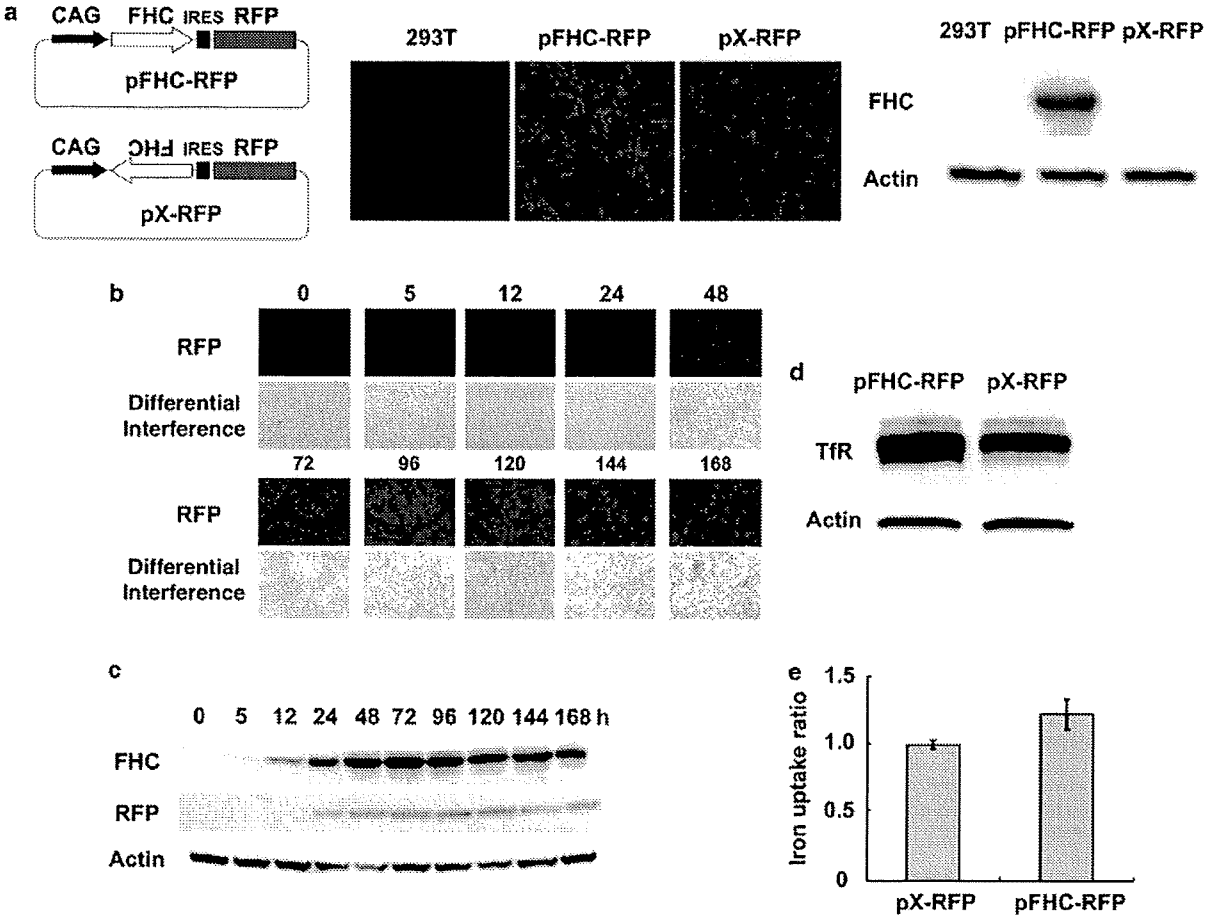

Figure 2 Dual-reporter protein expression in 293T cells and alterations of cellular iron metabolism. (a) Expression of dual-reporter proteins in 293T cells. Schema of a plasmid DNA construct carrying dual-reporter genes (pFHC–red fluorescence protein (RFP)) and a control plasmid carrying *RFP* gene and reversely inserted ferritin heavy chain (*FHC*) gene (pX-RFP) is shown. Non-transfected 293T cells showed no fluorescence signal. Cells transfected with the vectors showed red fluorescence on fluorescence microscopic images. Moreover, robust expression of FHC reporter protein in cells transfected with pFHC–RFP vector was confirmed by western blotting. (b) RFP expression in the pFHC–RFP vector-transfected cells. RFP fluorescence and differential interference images are shown. Times (hour) after transfection are indicated above the images. (c) Time course study of FHC and RFP expression confirmed nearly correlated transcription in the transfected cells. Times (hour) for sampling are indicated above the image. Actin was used as loading control. (d) Upregulation of transferrin receptor (TfR) in cells transfected with pFHC–RFP vector was noted. Actin was used as loading control. (e) FHC over-expressing cells augmented iron uptake. Results were obtained from 24-h incubation with ^{59}Fe. Radioactivity was counted from at least eight samples in two independent experiments and the counts were normalized by cell number. Mean ± s.d. IRES, internal ribosome entry site.

thereafter. The time course of FHC and RFP expression was examined in the pFHC–RFP-transfected cells using antibodies specific for each protein (Figure 2c). FHC expression appeared at 12 h, peaked at 72 h after transfection and slowly decreased. However, even 7 days (168 h) after transfection, FHC was still clearly detected. Consistent with the fluorescence microscopic images, RFP expression was first detected at 24 h and reached its maximum level at 96 h after transfection. Similar to FHC expression, RFP expression was also detectable at 7 days after transfection. It seemed that RFP was translated less efficiently than FHC, presumably because the expression of gene located downstream of IRES is often less efficient than that of its upstream gene.[34] Nevertheless, the RFP expression closely reflected the FHC expression, convincing us that monitoring the FHC expression would be sufficient. It has been reported that FHC overexpression induces TfR in the kidney of drug-inducible FHC transgenic mice.[35] We therefore evaluated TfR expression in cells with FHC reporter by western blotting. Consistent with the earlier result, TfR protein was increased in the cells with transient activation of FHC reporter compared with control cells (Figure 2d), suggesting that FHC reporter induces TfR upregulation. We then sought to determine whether FHC expression and its consequent upregulation of TfR altered the rate of iron influx in cells. It was found that iron uptake in cells with FHC reporter was increased by about 20% compared with reporter negative cells (Figure 2e). Taken together, these results suggest that our dual-reporter vector was functionally verified, and that activation of FHC reporter enhances iron uptake through TfR upregulation in cells.

Visualization of FHC reporter transgene expression by in vitro *MRI*

We conducted MRI of cell pellets to investigate the effects of FHC on the MR signal. Cells were transfected with

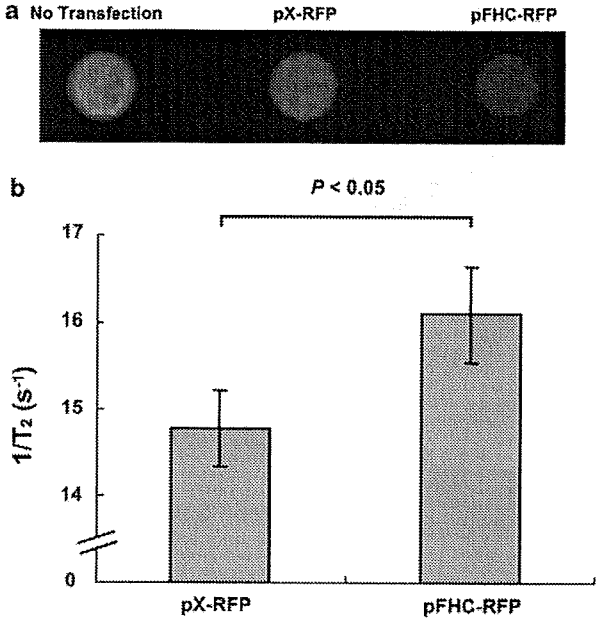

Figure 3 Cellular magnetic resonance imaging. (a) A representative T_2-weighted magnetic resonance imaging of transfected and non-transfected cell pellets. TR/TE = 4000/75 ms. Cells transfected with pFHC–red fluorescence protein (RFP) showed lower signal intensity compared with cells with pX-RFP. (b) For quantitative analysis, the transverse relaxation rate ($1/T_2$) of cell pellets was compared between cells with pX-RFP and those with pFHC–RFP, suggesting significant T_2 shortening by FHC reporter expression ($P < 0.05$). Mean ± s.d. ($n = 3$).

pFHC–RFP or pX-RFP and incubated with standard cell medium supplemented with iron for 3 days before MRI. Consistent with the earlier results,[29,30] the pFHC–RFP-transfected cells showed lower signal intensity in T_2-weighted MRI compared with pX-RFP-transfected control cells (Figure 3a). Quantitative analysis showed that the transverse relaxation rate ($1/T_2$) of the cells transfected with pFHC–RFP was significantly higher than that of control cells (Figure 3b), confirming that FHC expression shortens T_2 as we predicted.

In vivo *optical imaging and MRI of electroporation-mediated transgene expression in tumor*

To visualize the reporter transgene expression *in vivo* by optical imaging and MRI, we used 293T xenograft models and introduced naked pFHC–RFP or pRFP by *in vivo* EP. We carried out *in vivo* optical imaging and fluorescence stereoscopic microscopy before MRI. The information obtained from optical imaging ensured successful gene delivery and was helpful for the timing of MRI, enabling us to monitor the gene expression of FHC. Although RFP was expected to be less translated compared with FHC as mentioned above, we could readily detect RFP expression in tumor transfected with pFHC–RFP by both instrumentations (Figure 4a), and it was beneficial for choosing the MRI slices that covered the appropriate region where both reporters were expressed. In T_2-weighted MRI at 7 days after EP, tumors subjected to pRFP showed relatively homogeneous intensity, whereas tumors subjected to pFHC–RFP showed spotty but detectable hypo-intensity areas in the MRI slices (Figure 4b), showing that the ferritin MRI reporter system functions not only in a drug-inducible reporter system or highly efficient viral delivery system, but also in gene delivery with a relatively low transfection efficiency, such as *in vivo* EP. To validate the MRI results, the tumor was excised and carefully sectioned to obtain almost the same plane as seen on the MR image. RFP expression in the cross-section was observed correspondingly in the area showing low intensity in T_2WI (Figure 4c), suggesting that the T_2 change is attributable to the FHC reporter expression. For comparison of T_2-shortened areas in the tumors between RFP-tumor and FHC-tumor, we calculated mean T_2 in control RFP-tumors (57.6 ± 3.0 ms, see Materials and methods) and counted the number of pixels having a relaxation time below 51.6 ms (lower limit of two s.d. of mean T_2) in RFP-tumors and FHC tumors. This showed that the percentage of pixels showing T_2 shortening in FHC tumors was significantly increased compared with that in RFP-tumors (Figure 4d). These findings were consistent with the results of *in vitro* cellular MRI and strongly supported the notion that the hypo-intensity observed in *in vivo* T_2-weighted MRI resulted from FHC reporter expression.

Expression of both reporter proteins in FHC-transfected tumors

After *ex vivo* tumors were carefully sectioned to obtain a plane corresponding to an MRI-oriented image, we conducted fluorescence microscopic analysis and immunohistochemistry using antibodies specific for ferritin protein. RFP expression was clearly detected, with little or weak staining of ferritin being observed in RFP-tumor. In contrast, cells strongly stained by the antibody were observed in FHC-tumor, and they were well correlated with RFP-positive cells (Figure 5), confirming the correlation between RFP and FHC reporter expression.

In conclusion, we showed the dual modality of *in vivo* optical imaging and MRI of EP-mediated reporter transgene expression in experimental tumors. The method allowed us to visualize gene expression in samples with a broad scale from macroscopic to microscopic levels by using even a kind of plasmid vector. It is superior to other methods in respect to not needing to administer contrast agents and substrates, repetitive use capability and imaging at high spatial resolution. Our MRI detection using FHC reporter would be a clinically appropriate method for evaluating gene therapy mediated by *in vivo* EP even in cases of repeated protocol. Given that optical imaging and MRI are complementary in terms of high temporal resolution and sensitivity of the former and high spatial resolution of the latter, and that fluorescence imaging is evolving toward clinical application,[36] their combination may provide a new opportunity for evaluation of *in vivo* gene delivery to various tissues ranging widely from body surface to deep tissues in future clinical scenarios. In the gene therapy setting, if one connects the reporter genes to a therapeutic gene, the location, magnitude and duration of therapeutic gene co-expression with the reporter genes can be monitored non-invasively. Cancer gene therapy using *in vivo* EP has shown to be effective

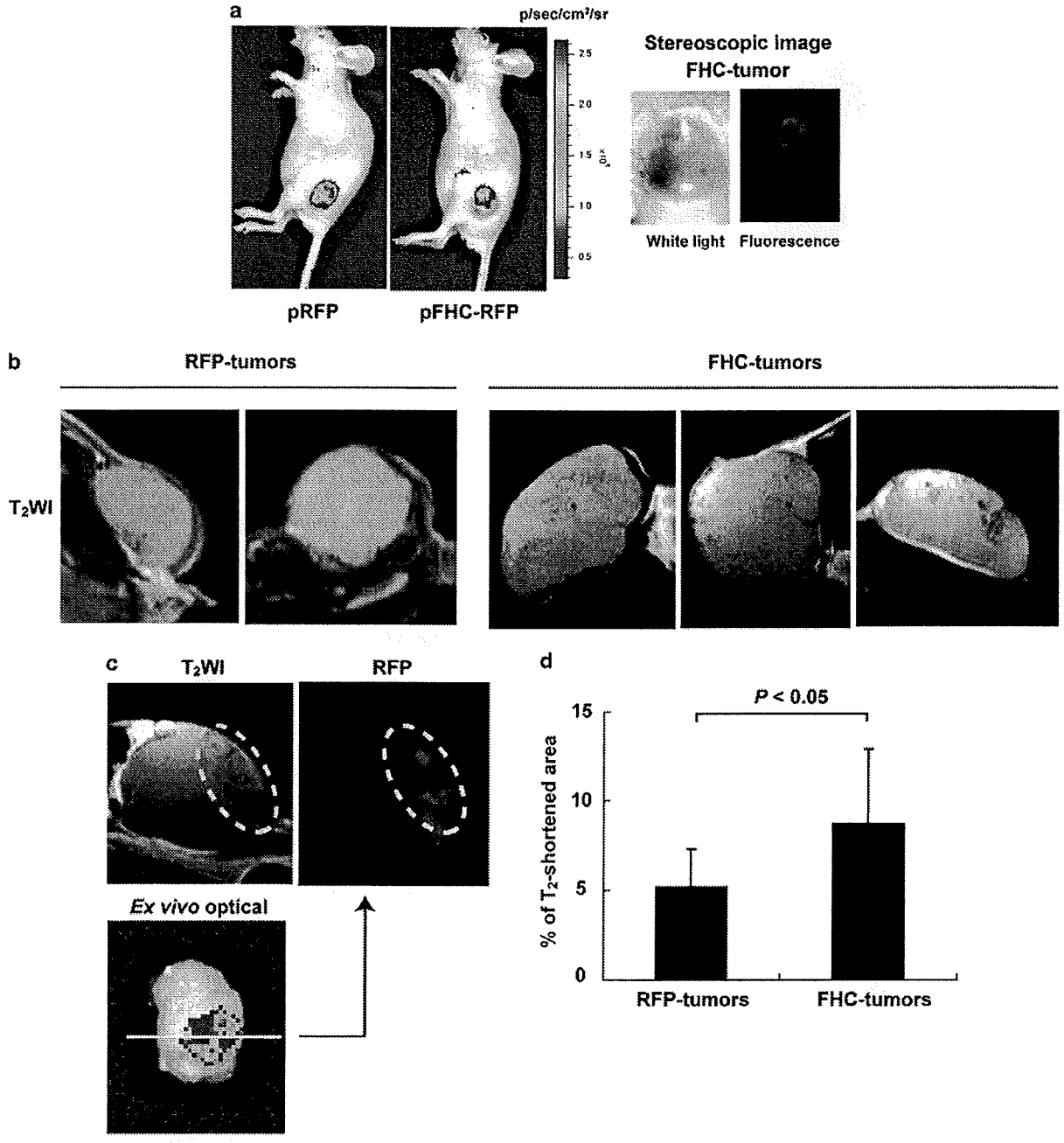

Figure 4 *In vivo* optical imaging and magnetic resonance imaging (MRI) of electroporation-mediated transgene expression. (a) Representative *in vivo* optical images of tumors transfected with pRFP or pFHC–red fluorescence protein (RFP) are shown. Stereoscopic fluorescence images of tumor transfected with pFHC–RFP (ferritin heavy chain (FHC)-tumor) conferred to the *in vivo* optical image showed a consistent light emission area. (b) Representative MRI T_2-weighted images (T_2WI) of tumors transfected with pRFP (RFP-tumors) or pFHC–RFP (FHC-tumors). Spotty low signal intensity areas were present in part of the FHC-tumors, whereas relatively homogeneous intensity was noted in RFP-tumors. TR/TE = 3000/50–60 ms. (c) Correlation between low-signal area in T_2WI and RFP expression in an FHC-tumor. A representative T_2WI of FHC-tumor and RFP expression in a cross-section derived from the same tumor are shown. Corresponding regions are surrounded by yellow dotted line. As a reference, *ex vivo* optical imaging of the tumor was also shown. The cross-section was obtained by dissection of *ex vivo* tumor at the white line with the aid of stereoscopic microscopy. (d) Comparison of T_2-shortened area between FHC-tumors and RFP-tumors. The percentage of pixels below the lower threshold limit (−2 s.d. of mean T_2 of RFP-tumors) was significantly increased in FHC-tumors ($P < 0.05$). Mean+s.d. ($n = 4$ for RFP-tumors, $n = 6$ for FHC-tumors).

in preclinical animal models, giving support to our approach. Although improvements to resolve the limitations of each modality are still needed, the 'proof-of-concept' approach we show in this report would be beneficial to the design of more efficient *in vivo* EP-mediated cancer gene therapy.

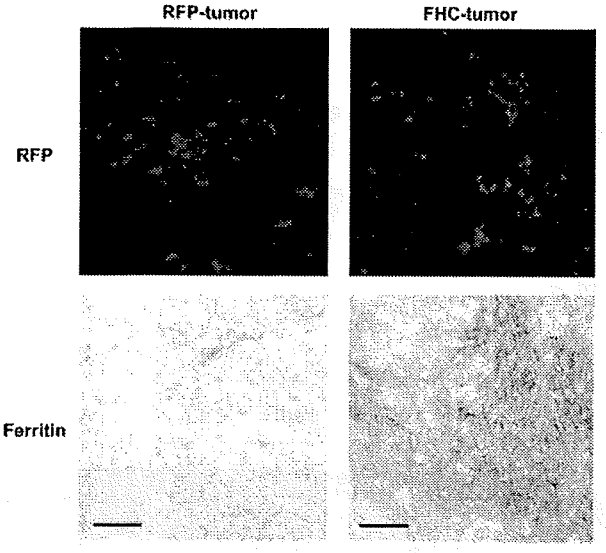

Figure 5 Expression of reporter proteins in a tumor section. Red fluorescence protein (RFP) and ferritin expression in the cryosection (7 μm) of a RFP- and a ferritin heavy chain-tumor. RFP was detected by fluorescence microscope and ferritin protein was stained by mouse anti-human ferritin antibody. Magnification, ×20. Scale bars = 50 μm.

Materials and methods

Cell lines

Human embryonic kidney 293T cells were cultured in DMEM (Sigma-Aldrich, St Louis, MO, USA) with 10% fetal bovine serum, 100 U ml^{-1} of penicillin and 100 μg ml^{-1} of streptomycin.

Plasmid

pRFP was constructed by insertion of DsRed-Express cDNA excised from pDsRed-Express (Clontech, Mountain View, CA, USA) into pCAGGS (kindly provided by Oriental Yeast Corp., Tokyo, Japan). For pFHC–RFP or pX-RFP, human FHC cDNA was cloned into a multiple cloning site of pIRES2-DsRed-Express (Clontech) at correct or reverse direction, respectively, and the resultant DNA fragment containing IRES and DsRed-Express was excised and ligated to pCAGGS.

Lipofection

The 293T cells were transfected with the vectors described above by Lipofectamine 2000 (Invitrogen Corp., Carlsbad, CA, USA) according to the manufacturer's instructions.

Western blotting

The procedures to detect FHC and RFP were described earlier.[32] In brief, cell lysates were separated on a 12.5% polyacrylamide gel and transferred to Immobilon-P membrane (MILLIPORE, Billerica, MA, USA). We used rabbit anti-human FHC antibody (Santa Cruz Biotechnology, Santa Cruz, CA, USA) or rabbit anti-DsRed antibody (Clontech) as a primary antibody for detection of FHC or RFP, respectively. In both cases, anti-rabbit IgG conjugated with horseradish peroxidase (GE Healthcare UK Ltd., Little Chalfont, UK) was used as a secondary antibody. For detection of TfR, total cell lysates were separated on a 7.5% polyacrylamide gel and transferred to Immobilon-P membrane. The blot was blocked by TBS BLOTTO A (Santa Cruz) at room temperature (RT) for 2 h and incubated with primary antibody at RT for 2 h. As a primary antibody, mouse anti-human TfR antibody (ZYMED, South San Francisco, CA, USA) was used at a concentration of 1 μg ml^{-1}. The membrane was washed three times with Tris-buffered saline containing 0.05% Tween 20, and incubated with an anti-mouse IgG conjugated with horseradish peroxidase (GE Healthcare). The blots were developed with ECL plus western blotting detection system (GE Healthcare). Images were obtained by Chemi-Smart 5000 (Vilber Lourmat, Marne-la-Vallée, France).

^{59}Fe uptake assay

The 293T cells were transfected with 1.6 μg of plasmid DNAs in a 12-well dish. One day after the transfection, $^{59}FeCl_3$ (Perkin Elmer, Boston, MA, USA) was added to the wells and incubated for 24 h. Cells were washed three times in phosphate-buffererd saline and radioactivity was measured by gamma counter (ALOKA, Tokyo, Japan). The counts were normalized by cell number.

Animal tumor model

The tumor xenograft model was developed by subcutaneous injection of 1×10^7 of 293T cells in 200 μl of Hanks' balanced salt solution (Invitrogen) in the lower back of nude mice (8–10-week-old female BALB/cA Jcl-nu/nu mice; CLEA, Tokyo, Japan). Tumor-bearing mice were subjected to *in vivo* EP when the tumor had reached an appropriate volume, mostly 75–150 mm^3 (usually 2 or 3 weeks after implantation). All animal model experiments were carried out in accordance with the guidelines for animal experimentation of the National Institute of Radiological Sciences.

In vivo *electroporation*

In vivo EP was carried out when tumors reached diameters of more than 5 mm. For all *in vivo* EP, we used a plate-and-fork-type electrode CUY663-5X8 (NEPA GENE, Ichikawa, Japan) and CUY21SC electoroporator (NEPA GENE) with constant electrical parameters. Detailed analysis of *in vivo* EP was described by Takei *et al*.[25] After anesthetizing the mouse, the fork-arm of the electrode was inserted into the undersurface of the tumor, the tumor was pinched by both arms and electrical resistance was measured and adjusted to below 1 KΩ, ideally 0.8–0.5 KΩ. Then, the plasmid DNA in phosphate-buffererd saline (80 μg/40 μl) was injected directly into the tumor by a 30-gauge needle, and EP was immediately carried out. Five electrical pulses were delivered with pulse length of 50 ms and 50 V field strength. In the second cycle, another five pulses with opposite polarity were administered. To reduce the electrical resistance of skin, the plate-arm surface was covered with an electrocardiogram pad.

In vivo *optical imaging*

Fluorescence light emission from tumors was monitored by IVIS lumina optical imaging system (Xenogen Corp., Alameda, CA, USA). Mice bearing xenograft tumors

were anesthetized by inhalation of 2.5% isoflurane and placed in a light-tight chamber. We selected the filter set for DsRed (excitation: 500–550 nm, emission: 575–650 nm, blue-shifted background excitation: 460–490 nm) and set the constant imaging parameters (exposure time: 2 s, binning: medium, lens aperture (f/stop): 2, field of view: 12.5 cm, floor lamp level: high). To obtain the autofluorescent-corrected image, the background filter image was subtracted from the primary excitation filter image using the Image Math tool and appropriate scale factor, according to the Living Image software version 2.6 (Xenogen Corp.) manual. The fluorescent area in the tumor, the region of interest, was encircled by hand, and the emission of light was quantified as photons per second. Then, the fluorescent area of *in vivo* tumor was re-confirmed by fluorescence stereoscopic microscope MZ16F (Leica Microsystem, Wetzlar, Germany).

Ex vivo *optical imaging*

Mice were killed and tumors were excised and stripped skin out. Optical images of *ex vivo* tumors were acquired using the IVIS imaging system with the same settings as described above in *in vivo* optical imaging, and also by fluorescence stereoscopic microscope MZ16F.

Fluorescence microscopy

Fluorescence from transfected cells or frozen sections of tumors was observed by Olympus FV1000 confocal laser microscopy system (Olympus, Tokyo, Japan), using a 543-nm excitation line and high-performance sputtered filter for DsRed or Olympus BX50 fluorescence microscope.

In vitro *MRI measurement*

The 293T cells were transfected with 8 μg of plasmid DNAs in a 60-mm dish. Cell medium was removed the next day, and 200 μM of ferric ammonium citrate in the standard medium was added every 24 h. After 72-h incubation with the iron supplementation, cells were washed, harvested, transferred to a 96-well PCR plate (INA OPTIKA, Osaka, Japan) and centrifuged. The 96-well PCR plate was cut to 6 × 6 matrix tubes and set on a cradle (made in-house) for stable and homogeneous MRI measurement. Proton MRI was carried out in a 7.0-T, 40-cm bore magnet (Jastec and Kobelco, Kobe, Japan) with 11.6-cm inner-diameter field gradient system (BGA-12, Bruker Biospin, Ettlingen, Germany) interfaced to a Bruker Avance console (Bruker). A 70-mm-diameter birdcage radio frequency coil (Bruker) for both transmitting and receiving was used. Multi-echo images were acquired 2 h after cell preparation using a spin-echo pulse sequence with pulse repetition time (TR) = 4000 ms, number of echoes = 16 (15–240, 15 ms increment), matrix = 128 × 128, FOV = 40 × 40 mm, slice thickness = 1 mm and in-plane resolution = 312.5 μm. We regarded the multi-echo images obtained by TE = 50–80 ms as T_2-weighted images. Slice orientation was horizontal, and it was adjusted to the cell pellets in the PCR tubes. Sample temperature was maintained at room temperature (~23 °C). Quantitative T_2 maps were calculated by a non-linear least-squares fitting using MRvision software (MRVision Co., Winchester, MA, USA) on Linux PC (Red Hat Linux, Mountain View, CA, USA). Region of interests were defined as precipitated cell regions. Mean ± s.d. of three independent samplings was used for statistical analysis.

In vivo *MRI measurement*

Mice bearing xenograft tumors were subjected to *in vivo* EP with pFHC–RFP or pRFP; gene expression was confirmed by optical imaging at 7 days after EP, and then MRI was conducted. The mice were anesthetized with 2.0% isoflurane, placed in a left or right lateral position and anesthesia was maintained at this level. During the experiment, a flow of warm air over the animal maintained body temperature at ~37.0 °C. Respiratory rate, monitored throughout the experiment, was maintained at 20–40 breaths per minute. *In vivo* MRI was acquired using the same 7.0-T magnet and field gradient system. The 70-mm-diameter birdcage radio frequency coil (Bruker) for transmitting and a saddle-shaped 2-channel phased array receiving surface coil (Rapid Biomedical, Rimper, Germany) were used. Multi-echo images were acquired using a spin-echo pulse sequence with TR = 3000 ms, number of echoes = 12 (10–120, 10 ms increments), matrix 256 × 256, FOV = 32 × 32 mm, slice thickness = 1 mm, in-plane resolution = 125 μm and slice gap = 1.2–1.8 mm. Slice orientation was transverse, and was localized in the tumor. Two adjacent transverse slices covering the area of RFP expression seen on the *in vivo* optical image were selected for generating quantitative T_2 maps. For tissue analysis on the T_2 maps, mean and s.d. of T_2 in the tumor was calculated out from all slices of RFP-transfected tumors. Then, the 'T_2-shortened area' was defined as pixels that were below the threshold level as −2 s.d. of the mean T_2. Percentages of the 'T_2-shortened area' of the entire tumor area in the plane were calculated and compared between the RFP-transfected and FHC-transfected tumor.

Immunohistochemistry

Tumors subjected to EP were excised after MRI and the orientation of the transfected areas was re-checked with the aid of fluorescence stereoscopic microscopy. The tumor specimens were embedded in OCT compound and sectioned in the same direction as MRI into 7-μm thick slices. Cryosections were fixed in 4% paraformaldehyde phosphate buffer solution (Wako, Osaka, Japan). Immunohistochemistry was done using the Vector M.O.M peroxidase immunodetection kit and ImmPACT DAB substrate (Vector Laboratories, Burlingame, CA, USA) in accordance with the manufacturer's instructions. We used a mouse monoclonal antibody against human ferritin (0.5 μg ml^{-1}, BMA Biomedicals, Augst, Switzerland) as primary antibody.

Statistical analysis

Significance of differences was determined by Student's *t*-test. *P*-values <0.05 were considered significant.

Conflict of interest

The authors declare no conflicts of interest.

Acknowledgements

We thank Dr Paolo Arosio (University of Brescia, Italy) for the generous gift of ferritin cDNA; Dr Jun-ichi Miyazaki (Osaka University, Japan) for the generous donation of pCAGGS vector; Kosho Suzuki (NEPA GENE) for technical suggestions for *in vivo* EP; Michiko Narazaki, Misao Yoneyama, Sayaka Shibata and Shigeyoshi Saito for skillful assistance with the MRI experiments; Hikaru Takenaka for preparation of the paper; members in our group for helpful discussions; Drs Yasuhito Sasaki, Yoshiharu Yonekura and Shuji Tanada for encouragements for this study. This study was supported in part by a Grant-in-Aid for Scientific Research for Exploratory Research from the Ministry of Education, Culture, Sports, Science and Technology, Japan (18659357: S Hasegawa); Intramural Research Grant from the National Institute of Radiological Sciences (S Hasegawa).

References

1 Alexander BL, Ali RR, Alton EW, Bainbridge JW, Braun S, Cheng SH *et al.* Progress and prospects: gene therapy clinical trials (part 1). *Gene Therapy* 2007; **14**: 1439–1447.
2 Aiuti A, Bachoud-Levi AC, Blesch A, Brenner MK, Cattaneo F, Chiocca EA *et al.* Progress and prospects: gene therapy clinical trials (part 2). *Gene Therapy* 2007; **14**: 1555–1563.
3 Porteus MH, Connelly JP, Pruett SM. A look to future directions in gene therapy research for monogenic diseases. *PLoS Genet* 2006; **2**: e133.
4 Payen E, Bettan M, Rouyer-Fessard P, Beuzard Y, Scherman D. Improvement of mouse beta-thalassemia by electrotransfer of erythropoietin cDNA. *Exp Hematol* 2001; **29**: 295–300.
5 Argyros O, Wong SP, Niceta M, Waddington SN, Howe SJ, Coutelle C *et al.* Persistent episomal transgene expression in liver following delivery of a scaffold/matrix attachment region containing non-viral vector. *Gene Therapy* 2008; **15**: 1593–1605.
6 Daud AI, DeConti RC, Andrews S, Urbas P, Riker AI, Sondak VK *et al.* Phase I trial of interleukin-12 plasmid electroporation in patients with metastatic melanoma. *J Clin Oncol* 2008; **26**: 5896–5903.
7 Shimao K, Takayama T, Enomoto K, Saito T, Nagai S, Miyazaki J *et al.* Cancer gene therapy using *in vivo* electroporation of Flt3-ligand. *Int J Oncol* 2005; **27**: 457–463.
8 Kaiga T, Sato M, Kaneda H, Iwakura Y, Takayama T, Tahara H. Systemic administration of IL-23 induces potent antitumor immunity primarily mediated through Th1-type response in association with the endogenously expressed IL-12. *J Immunol* 2007; **178**: 7571–7580.
9 Golzio M, Mazzolini L, Ledoux A, Paganin A, Izard M, Hellaudais L *et al. In vivo* gene silencing in solid tumors by targeted electrically mediated siRNA delivery. *Gene Therapy* 2007; **14**: 752–759.
10 Isaka Y, Imai E. Electroporation-mediated gene therapy. *Expert Opin Drug Deliv* 2007; **4**: 561–571.
11 Goto T, Nishi T, Tamura T, Dev SB, Takeshima H, Kochi M *et al.* Highly efficient electro-gene therapy of solid tumor by using an expression plasmid for the herpes simplex virus thymidine kinase gene. *Proc Natl Acad Sci USA* 2000; **97**: 354–359.
12 Lohr F, Lo DY, Zaharoff DA, Hu K, Zhang X, Li Y *et al.* Effective tumor therapy with plasmid-encoded cytokines combined with *in vivo* electroporation. *Cancer Res* 2001; **61**: 3281–3284.
13 Tamura T, Nishi T, Goto T, Takeshima H, Dev SB, Ushio Y *et al.* Intratumoral delivery of interleukin 12 expression plasmids with *in vivo* electroporation is effective for colon and renal cancer. *Hum Gene Therapy* 2001; **12**: 1265–1276.
14 Lucas ML, Heller L, Coppola D, Heller R. IL-12 plasmid delivery by *in vivo* electroporation for the successful treatment of established subcutaneous B16.F10 melanoma. *Mol Ther* 2002; **5**: 668–675.
15 Matsubara H, Mizutani Y, Hongo F, Nakanishi H, Kimura Y, Ushijima S *et al.* Gene therapy with TRAIL against renal cell carcinoma. *Mol Cancer Ther* 2006; **5**: 2165–2171.
16 Massoud TF, Gambhir SS. Molecular imaging in living subjects: seeing fundamental biological processes in a new light. *Genes Dev* 2003; **17**: 545–580.
17 Golzio M, Rols MP, Gabriel B, Teissie J. Optical imaging of *in vivo* gene expression: a critical assessment of the methodology and associated technologies. *Gene Ther* 2004; **11**(Suppl 1): S85–S91.
18 Inubushi M, Wu JC, Gambhir SS, Sundaresan G, Satyamurthy N, Namavari M *et al.* Positron-emission tomography reporter gene expression imaging in rat myocardium. *Circulation* 2003; **107**: 326–332.
19 Serganova I, Blasberg R. Reporter gene imaging: potential impact on therapy. *Nucl Med Biol* 2005; **32**: 763–780.
20 Furukawa T, Lohith TG, Takamatsu S, Mori T, Tanaka T, Fujibayashi Y. Potential of the FES-hERL PET reporter gene system—basic evaluation for gene therapy monitoring. *Nucl Med Biol* 2006; **33**: 145–151.
21 Siddiqui F, Barton KN, Stricker HJ, Steyn PF, Larue SM, Karvelis KC *et al.* Design considerations for incorporating sodium iodide symporter reporter gene imaging into prostate cancer gene therapy trials. *Hum Gene Ther* 2007; **18**: 312–322.
22 Niwa H, Yamamura K, Miyazaki J. Efficient selection for high-expression transfectants with a novel eukaryotic vector. *Gene* 1991; **108**: 193–199.
23 Brooks AR, Harkins RN, Wang P, Qian HS, Liu P, Rubanyi GM. Transcriptional silencing is associated with extensive methylation of the CMV promoter following adenoviral gene delivery to muscle. *J Gene Med* 2004; **6**: 395–404.
24 Maruyama H, Ataka K, Higuchi N, Sakamoto F, Gejyo F, Miyazaki J. Skin-targeted gene transfer using *in vivo* electroporation. *Gene Therapy* 2001; **8**: 1808–1812.
25 Takei Y, Nemoto T, Mu P, Fujishima T, Ishimoto T, Hayakawa Y *et al. In vivo* silencing of a molecular target by short interfering RNA electroporation: tumor vascularization correlates to delivery efficiency. *Mol Cancer Ther* 2008; **7**: 211–221.
26 Pedron-Mazoyer S, Plouet J, Hellaudais L, Teissie J, Golzio M. New anti angiogenesis developments through electro-immunization: optimization by *in vivo* optical imaging of intradermal electro gene transfer. *Biochim Biophys Acta* 2007; **1770**: 137–142.
27 Bloquel C, Trollet C, Pradines E, Seguin J, Scherman D, Bureau MF. Optical imaging of luminescence for *in vivo* quantification of gene electrotransfer in mouse muscle and knee. *BMC Biotechnol* 2006; **6**: 16.
28 Heller LC, Ugen K, Heller R. Electroporation for targeted gene transfer. *Expert Opin Drug Deliv* 2005; **2**: 255–268.
29 Genove G, DeMarco U, Xu H, Goins WF, Ahrens ET. A new transgene reporter for *in vivo* magnetic resonance imaging. *Nat Med* 2005; **11**: 450–454.
30 Cohen B, Dafni H, Meir G, Harmelin A, Neeman M. Ferritin as an endogenous MRI reporter for noninvasive imaging of gene expression in C6 glioma tumors. *Neoplasia* 2005; **7**: 109–117.
31 Cohen B, Ziv K, Plaks V, Israely T, Kalchenko V, Harmelin A *et al.* MRI detection of transcriptional regulation of gene expression in transgenic mice. *Nat Med* 2007; **13**: 498–503.

32 Aung W, Hasegawa S, Furukawa T, Saga T. Potential role of ferritin heavy chain in oxidative stress and apoptosis in human mesothelial and mesothelioma cells: implications for asbestos-induced oncogenesis. *Carcinogenesis* 2007; **28**: 2047–2052.
33 Gilad AA, Winnard Jr PT, van Zijl PC, Bulte JW. Developing MR reporter genes: promises and pitfalls. *NMR Biomed* 2007; **20**: 275–290.
34 Ngoi SM, Chien AC, Lee CG. Exploiting internal ribosome entry sites in gene therapy vector design. *Curr Gene Ther* 2004; **4**: 15–31.
35 Wilkinson JT, Di X, Schonig K, Buss JL, Kock ND, Cline JM *et al*. Tissue-specific expression of ferritin H regulates cellular iron homoeostasis *in vivo*. *Biochem J* 2006; **395**: 501–507.
36 Weissleder R, Pittet MJ. Imaging in the era of molecular oncology. *Nature* 2008; **452**: 580–589.